Available online at www.sciencedirect.com
SCIENCE DIRECT®
Coordination Chemistry Reviews 249 (2005) 2649–2660
COORDINATION CHEMISTRY REVIEWS
www.elsevier.com/locate/ccr

Review

Spin density distribution in transition metal complexes

Eliseo Ruiz, Jordi Cirera, Santiago Alvarez *

Departament de Química Inorgànica and Centre Especial de Recerca en Química Teòrica, Universitat de Barcelona, Martí i Franqués 1-11, 08028 Barcelona, Spain

Received 8 February 2005; accepted 14 April 2005
Available online 11 July 2005

Contents

Abstract

The computational approaches that can be used to calculate the spin density distribution in transition metal compounds are discussed, the characteristic trends involving spin delocalization and spin polarization mechanisms are summarized, and the characteristic shapes of the spin density distributions around a transition metal atom are presented. Reference is also made to experimental methods to determine spin density distributions and to incipient work in the field of high spin molecules and single-molecule magnets.

Keywords: Spin density; Spin polarization; Spin delocalization; Exchange coupling

1. Introduction

The distribution of the unpaired spin density has long been recognized to be important in determining the NMR isotropic shift of the different nuclei in paramagnetic molecules [1–5]. NMR spectra, however, are only sensitive to the electron spin density at the nucleus and provide information only on that part of the spin density associated with the s orbitals. The hyperfine coupling of the electron spin density with nuclear spin has traditionally been detected in the EPR spectra. In that case, comparison of the isotropic and anisotropic hyperfine coupling is needed in order to obtain the sign of the spin density [6]. Another technique that provides information of the spin density distribution is the polarized neutron diffraction (abbreviated in what follows as PND). Such data can be fitted to a set of atomic orbitals at various levels of sophistication. The validity of the method has been critically discussed and other methods are available that do not introduce an a priori theoretical model to fit the experimental data, such as the so-called magnetic wave function modeling [7] or the maximum entropy method [8]. The atomic spin density can also be determined by X-ray magnetic circular dichroism (XMCD), a technique that has been mainly employed in solid state compounds and alloys [9], although applications to a Mn(II)–Cu(II) chain compound and a dodecanuclear Mn compound have been recently reported [10,11].

* Corresponding author. Tel.: +34 934021269; fax: +34 934907725.
E-mail address: santiago@qi.ub.es (S. Alvarez).

0010-8545/$ – see front matter © 2005 Elsevier B.V. All rights reserved.
doi:10.1016/j.ccr.2005.04.010

A renewed interest in the study of spin density distribution has bloomed in recent years because its understanding is foreseen as a useful tool for the design of ferro- or antiferromagnetic interactions between paramagnetic centers in polynuclear systems. Recent accounts of spin density distributions in transition metal complexes obtained through PND [12] and NMR [13] experiments have been published, and an earlier review paper revised the conceptual aspects of spin density distribution in transition metal complexes [14]. Thus, in this paper we will briefly summarize the spin distribution mechanisms, then we will discuss some practical aspects of the computation of spin densities, and finally will describe the main shapes that the spin distribution around the metal atoms is expected to present. When discussing spin densities we must note first the sign convention, since both positive and negative values of the spin density can be found. We adopt the usual convention that the electron density associated with a spin aligned parallel to the applied field (up-magnetization in PND) is taken as positive, and that corresponding to antiparallel spin (down-magnetization in PND) as negative.

2. Computation of spin densities

Several approaches can be used to calculate the spin density distribution in a coordination compound. The presence of transition metal atoms makes it particularly useful to use theoretical methods based on density functional theory due to the direct inclusion of the correlation effects [15]. The use of simple exchange-correlation functionals, in both the local and generalized gradient-approximation (GGA) formulations, provides a qualitative picture of the system, although such methods predict too large a delocalization of the spin. The use of hybrid methods that combine an exchange-correlation functional with some exact exchange contributions corrects this drawback. Let us consider as a benchmark case the $[Ni(H_2O)_6]^{2+}$ complex. For this compound, the LDA [16,17] and BLYP [18,19] functionals give a Mulliken spin population at the Ni atom of 1.631 and 1.669, respectively, whereas the value obtained with the B3LYP [20] functional is 1.760, much closer to the PND experimental value of 1.770 [21]. Due to the neglect of correlation contributions, the UHF method overestimates the spin localization resulting in a value of 1.902. Ressouche and Schweizer, in a study of organic free radicals, also concluded that density functional methods are far superior than UHF for reproducing the experimental spin densities [22]. The second important choice is the population analysis scheme used to calculate the spin density. Usually, the Mulliken population analysis has been employed, but this population analysis scheme presents well-known problems that can be specially seen in the calculated atomic charges (Table 1, note the highly negative charge of the Cr atom). Hence, alternative methods such as those based on the natural bond orbitals (NBO) [23] or atoms in molecules (AIM) [24] approaches are often employed. It is worth stressing that the calculation of the spin density is much less sensitive to the choice of the population analysis scheme than the atomic charges (Table 1). The AIM approach, in spite of its higher computational demand, does not give significantly better results as compared to experimental PND data, as seen in the model example of Table 1 and in more realistic systems found in the literature [25,26]. In summary, a fair description of the spin distribution pattern in a molecule can be expected regardless of the method of population analysis employed, as compared to the experimental PND data, although the NBO scheme seems to provide to most reliable results from the numerical point of view [27].

Table 1
Calculated spin populations and atomic charges for $[Cr(CN)_6]^{3-}$ using three different approaches, Mulliken, natural bond orbital (NBO) and atoms in molecules (AIM) population analysis with the B3LYP functional [20] and a triple-ζ basis set [52]

	Mulliken	NBO	AIM	Experimental
Atomic charge				
Cr	−1.040	+0.305	+1.629	
C	−0.056	+0.080	+0.431	
N	−0.268	−0.632	−1.205	
Spin population				
Cr	+3.304	+3.007	+2.772	+3.250
C	−0.138	−0.074	−0.030	−0.087
N	+0.087	+0.073	+0.068	+0.045
r.m.s.	0.171	0.069	0.296	

The experimental PND data [27] and the root mean square deviations are provided for comparison.

Another important aspect of the calculations is the choice of the basis set. In principle, we expect the spin density for the core orbitals to be negligible, regardless of the DFT method and population analysis scheme used. However, even if not much exploration of the effect of pseudopotentials on the calculated spin densities has been carried out, Liu has reported calculations that show non-negligible variations in the Fe spin density in iron porphyrin [28]. Work in progress in our group shows that the effects of using pseudopotentials on calculated spin densities can be larger than those reported by Liu and apparently erratic. The use of pseudopotentials has also been shown to affect the calculated values of exchange coupling constant in polynuclear complexes [29]. Therefore, spin densities obtained with basis sets that replace the core electrons by pseudopotentials, as happens for most plane wave or numerical basis sets, should be taken with caution. Other than that, the calculated spin densities are relatively insensitive to the quality of the basis set. Thus, for instance, using a Mulliken analysis with a double-ζ basis set [30], the spin population of Cr in $[Cr(CN)_6]^{3-}$ is +3.150, relatively close to the value presented in Table 1 for a triple-ζ basis set (+3.304). Again, the calculated charges are much more sensitive than the spin density to the choice of basis set, as seen by comparing the Mulliken charges for Cr with double-ζ (+0.577) and triple-ζ (−1.040) basis sets. We must conclude that a correct description of the spin density can be obtained by using a hybrid functional, and that the choice of the population analysis and basis set does not play a crucial

role to obtain a correct semi-quantitative picture of the spin distribution.

Most of the spin density distribution data, both experimental and computational, can be understood qualitatively in simple terms, by taking into account the theoretical foundations of the two electron interactions that determine the spatial distribution of α and β electrons in a paramagnetic molecule. The main concepts are summarized in the following section.

3. Spin distribution in metal complexes

3.1. General rules for mononuclear complexes

There are two mechanisms through which an unpaired d electron of a transition metal ion can place some spin density at the other atoms of the molecule, as well as at its own other atomic orbitals. On one hand, the molecular orbital that hosts an unpaired electron, even if with major contribution from the metal d orbital, mixes in the atomic orbitals of the ligands, mostly from the donor atoms. Therefore, the probability of finding the unpaired electron at a particular atomic orbital χ_μ is related to the square of the coefficient $c_{i\mu}$ with which that AO participates in the *i*th singly occupied molecular orbital (SOMO). Since we adopt the convention that the unpaired electron has a positive spin, its delocalization results in a distribution of positive spin density throughout the molecule determined by the composition of the SOMO. The resulting distribution of spin density is said to arise from a spin delocalization mechanism. Summing up the spin densities of the different atomic orbitals of one atom, one obtains the corresponding atomic spin density. Some rules of thumb can be recalled at this point, deduced from our knowledge of orbital interaction rules: (i) the spin density delocalization is more important for the atoms directly bound to the paramagnetic center; (ii) the amount of spin delocalization increases with the covalent character of the metal–ligand bond; (iii) the delocalization of spin density for σ-type orbitals (e.g., those in e_g orbitals of octahedral complexes) is much more important than for π-type ones (e.g., the t_{2g} orbitals in octahedral complexes).

The second way, through which the positive spin at the paramagnetic center may induce some spin density of the opposite sign at the atoms bonded to it, is the spin polarization mechanism. It is the result of the exchange term introduced by the Pauli principle, that favors the probability of finding two electrons of identical spin in the same region of space (in much the same way that Hund's rule for atoms predicts the term with the highest spin multiplicity to have the lowest energy). Therefore, the spin of a bonding electron pair is polarized, in such a way that the positive spin is concentrated close to the atom that has an unpaired electron, whereas a concentration of negative spin density is favored around the atoms bonded to it. This effect propagates through the molecule away from the paramagnetic center, thus generating spin densities of alternating sign at rather long distances. The net spin density at a particular AO or atom therefore results from the combination of the two mechanisms that can add up to give a positive value (when both mechanisms contribute a positive spin density) or compensate in part to give either a small positive (delocalization mechanism predominant) or negative (spin polarization predominant) total spin density. We must notice here that spin polarization importantly affects also the paired electrons at the paramagnetic centers, such as the t_{2g} electrons in the Ni(II) octahedral complexes with two unpaired electrons in the e_g orbitals [14], as schematically shown in **1**, where the α and β spin-orbitals of the M–L bonding orbital are mostly centered at the metal and donor atom, respectively.

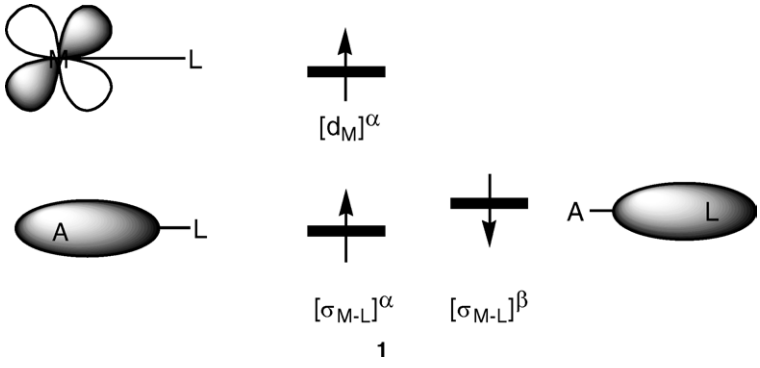

1

In complexes with *n* unpaired electrons in the valence molecular orbitals centered mainly at the metal atom, a total spin density of +*n* should be expected for those molecular orbitals (the SOMOs). A large portion of the spins can be ascribed to the metal d atomic orbitals, because they present the major contributions to the SOMOs, although some spin density is delocalized to the ligands and the spin population at the metal is often less than the number of electrons. The difference between the number of unpaired electrons and the total spin density at the metal atom should then be taken as a measure of the degree of covalent character of the metal–ligand bonds, that follows the nephelauxetic series. In octahedral complexes, delocalization toward the ligands is more important for the σ-type e_g than for the π-type t_{2g} orbitals, and the deviation of the spin density from the number of unpaired electrons is always larger for the former. Comparison of similar complexes down a transition group shows that the spin delocalization is larger for the metals of the second and third

transition series than for the corresponding metal of the first transition series. Exceptions to the positive spin delocalization to the donor atoms correspond to complexes with the most electronegative F or O donor atoms when the unpaired electrons are in a π-type (t_{2g}) molecular orbital.

For those electron configurations with both unpaired and paired electrons in the metal d orbitals, the electron pairs are spin polarized and therefore carry a small amount of net positive spin. Similarly, the formally empty d orbitals, such as the e_g ones in a $t_{2g}^3 e_g^0$ configuration, carry some positive spin density due to the polarization of the electron pair in a low-lying bonding molecular orbital centered mainly on the ligands. The placement of spin density at the formally empty atomic orbitals of the metal atom due to spin polarization seems to be more important for the d than for the s and p orbitals. It has also been found that the importance of the spin density at a given atomic orbital resulting from spin polarization is roughly proportional to the number of unpaired electrons at the metal atom.

When the unpaired electrons at the metal atom are strongly localized, as for t_{2g}^n configurations in complexes with σ-donor ligands, the spin density at the metal atom can be larger than the number of unpaired electrons due to spin polarization of the bonding electron pairs.

As a general rule, the combination of spin delocalization and spin polarization results in a spin density distribution such as that shown in **2**. The donor atoms directly attached to the metal carry positive spin density, and from there on the spin density is propagated through the bonds of the ligand with alternating signs. Exceptions to this rule are to be expected when delocalization is important beyond the donor atom, a situation that occurs in the presence of important π metal–ligand interactions involving unpaired t_{2g} electrons. An example of such a situation is given by cyano ligands, for which mixing of the t_{2g} metal orbital with its π and π^* orbitals results in larger delocalization to the N than to the C atom and induces a net positive spin density at the nitrogen atoms. Since the carbon atoms experience no spin delocalization, all their atomic orbitals are spin-polarized and carry a negative spin density.

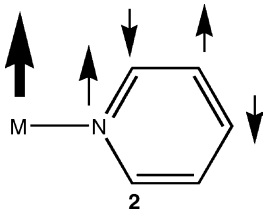

2

It must be borne in mind that spin density data coming from NMR experiments results from the hyperfine coupling of the electronic and nuclear spins and is reflects only unpaired electrons at the ns orbitals, which are the only ones that do not have a node at the nuclear position. Therefore, we should not expect good quantitative agreement between the calculated and experimental NMR atomic spin densities. Furthermore, comparison of only s atomic orbital spin density with the NMR data is likely to require the use of an all electron basis set, to take into account the spin polarization of the inner s electrons that is likely to have significant participation in the hyperfine coupling.

3.2. Examples of dinuclear complexes

For an azido-bridged dinuclear complex, $[Cu_2(\mu\text{-}N_3)_2(4\text{-}{}^t\text{Bupy})_4](ClO_4)_2$ (4-^{t}Bupy = *para–tert*-butylpyridine), Kahn et al. determined the spin density maps from polarized neutron diffraction studies [31]. The atomic spin densities obtained from B3LYP calculations for the triplet state [32] seem to overestimate the spin delocalization, giving smaller spin densities at the copper atom. The use of the "atoms in molecules" analysis proposed by Bader [24] in model calculations results in better agreement with the experimental spin density than Mulliken or NBO population analysis schemes in this case. The spin densities at the bridging and terminal nitrogen atoms of the azido bridge have the same sign as in the copper atoms, both from experiment and from calculations, indicating that spin delocalization toward the donor atoms predominates over the polarization mechanism for this system [14]. The sign alternation of the spin density at the N2 and N3 atoms of the azido bridge is consistent with spin polarization by the bridging nitrogen atoms. However, the spin distribution scheme may vary when changing the metal atom, from Cu(II) to Ni(II) to Mn(II). The delocalization of the unpaired electrons at the e_g-type orbitals toward the donor atoms decreases along the series Cu > Ni > Mn, while the spin polarization increases in the same direction, due to the increased number of unpaired electrons. As a result, the spin density is positive at the terminal donor atoms and positive at the bridging atoms for Cu and Ni, but small and negative for Mn.

A study of the spin density distribution in dinuclear Cu(II) complexes with bridging ligands having the same topology (**3**, where WH, X. Y and ZH can be O, S or NH) as the oxalate anion [33] showed that spin delocalization to the donor atoms decreases with their increasing electronegativity, but the combined spin density at the Cu and donor atoms is practically constant and the spin density at the terminal ligands is practically independent on the substitution pattern of the bridging ligand. An exception to this behavior is found in the bisimidazole and bipyrimidine bridges, in which a significant amount of spin density is delocalized throughout the aromatic rings. On the other hand, when the donor positions are occupied by NH groups, the spin density at the donor atom is significantly affected by the orientation of the hydrogen atom, increasing with the angle φ (**3**) The spin densities at the central carbon atoms of the bridging ligands are rather small and negative (less than 0.01 in absolute value, compared to values between 0.06 and 0.12 at the donor atoms), indicating that the spin delocalization and spin polarization mechanisms approximately cancel out. It is worthy of note that the antiferromagnetic character of the exchange coupling in these dinuclear complexes increases with decreasing spin density

at the copper atoms. Relationship between spin density at the metal atoms and exchange coupling constants have also been analyzed for cyano-bridged dinuclear complexes [40].

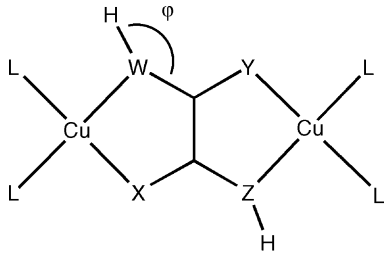

3

A combined PND and DFT study of the bimetallic chain compound $[MnNi(NO_2)_4(en)_2]$, whose repeat unit is shown in **4**, allowed us [34] to (a) calibrate the ability of the computational method to match the experimental results, (b) test the performance of different population analysis schemes, (c) study the effect of modeling the chain by a binuclear complex on the calculated spin densities and (d) analyze the changes in spin density distribution on going from a mono- to a dinuclear complex. Very good agreement, even at the quantitative level, was obtained between the calculated atomic spin densities and the corresponding PND values. In contrast with what was found for the azido-bridged complex discussed above, the results were somewhat poorer with the AIM population analysis than with the NBO or Mulliken schemes, with the latter giving the best match between experiment and theory. The nitrito-bridged chain was modeled by a binuclear complex in two different ways, either by saturating the pending bonds (represented by stripes in **4**) with protons, or by just disconnecting the coordination bonds between the monomer and the rest of the chain, leaving the corresponding nitrito groups as terminal ligands. It was found that both models yield good agreement with experiment, although the un-protonated model gave slightly better results. In contrast, these two models are not so good in calculating the exchange coupling constant, resulting in being too ferromagnetic for the protonated model and a bit too antiferromagnetic for the nude model, consistent with the fact that the missing metal atoms in these models are weaker Lewis acids than the proton. Comparison of the atomic spin densities in this complex with those in the mononuclear parent compounds indicates that the atomic spin densities in the chain model are practically the sum of those in the mononuclear precursors.

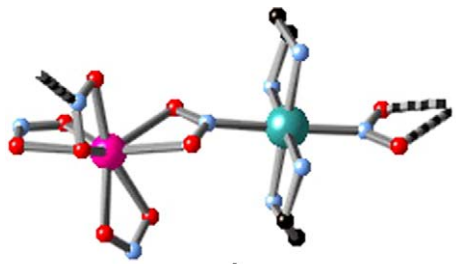

4

In a Ti(IV) complex with diquinone radical ligands, spin delocalization works in the opposite direction compared to typical complexes in which the unpaired electrons are sitting at the metal atoms. Here, the unpaired electrons belong to the ligands and the formally d^0 Ti atom obtains significant spin density by delocalization, according to PND experiments and DFT calculations [35].

4. Spin density shapes

In the last decades, much research has been devoted to the elucidation of the shape of the electron density of molecules, both from theory and from X-ray diffraction data. However, the contributions from the core, bonding and non-bonding valence electrons to the total electron density cannot be sorted out. Since the electron density comes mostly from the core electrons, specially for heavy atom systems, information from valence electrons (those responsible for the chemical, optical and magnetic properties) has to be inferred from the analysis of the Laplacian of the electron density [24]. On the other hand, there is an increasing interest in finding experimentally the shape of the probability distribution of individual electrons or pairs of electrons, in an attempt to verify whether the shape of the molecular orbitals obtained from theory is just a consequence of the use of atomic orbitals as basis functions and not a fundamental property of matter subject to experimental validation. In the most recent attempt in such direction, Itatani et al. have reported the "photograph" of the σ_g lone pair molecular orbital of N_2 by means of tomographic imaging, using high harmonics generated from intense femtosecond laser pulses focused on aligned molecules [36].

In contrast to the electron density, the spin density distribution maps the tridimensional shape of the single occupied molecular orbitals (SOMOs). Therefore, the shape of the spin density, obtained very easily from calculations, can in principle be determined also experimentally through the techniques mentioned above, even if currently the theoretical approach gives a more detailed description, while the experimental data typically offers resolution at the atomic scale only or is given as a contour plot in a section of the molecule. For that reason, it is timely to discuss the basic shapes to be expected around the metal atom in transition metal complexes, which is the object of this section. To that end, we show here the spin densities of complexes with the simplest ligand (the σ-donor hydride) in tetrahedral and octahedral geometries having selected electron configurations. Then we will show a couple of examples of di- and polynuclear systems in which these simple patterns are reproduced.

We start by looking at mononuclear complexes with only one unpaired electron. In an octahedral complex with the t_{2g}^1 electron configuration, in which the unpaired electron is strictly located in a metal d orbital because interaction with the orbitals of the σ-donor ligands is forbidden by symmetry, the shape of the electron density naturally reproduces that

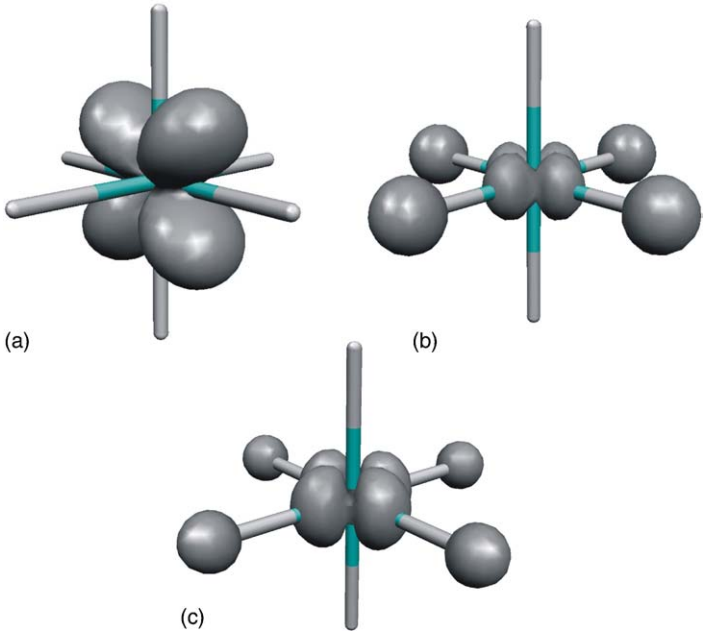

Fig. 1. Representation of the isodensity surfaces (cutoff of 0.02) of the spin density distribution for octahedral d^1 (a) and d^9 (b) complexes calculated using a gaussian orbital basis set. The same representation for the d^9 case calculated with a plane waves basis set (c) is also shown. Gray shapes correspond to positive spin densities.

of a d orbital (Fig. 1a). The d orbital shape appears also in a complex with the $t_{2g}^6 e_g^3$ configuration (Fig. 1b), supplemented with positive spin density regions around at the ligands' positions, an expected result due to the mixing of metal and ligand contributions in the e_g molecular orbitals. The shape of the spin density at the selected cutoff value of Fig. 1, with empty regions between the positive spin accumulations centered at the metal and ligands, point to the existence of minima in the spin density distribution along the metal–ligand bonds. In other words, the spin density distribution corresponding to antibonding SOMOs present (3, −1) critical points akin to those that the total electron densities show for chemical bonds [24] (see discussion for the $t_{2g}^6 e_g^3$ case below).

At this point it is appropriate to ask whether the d-orbital shape of the spin density is just an artifact associated with the use of an orbital basis set. Such question can be answered by calculating the spin density distribution of the same compound using plane waves instead of orbitals as a basis set [38]. A recently reported result [29] clearly confirms that the four-lobed shape (shown for our simplified model in Fig. 2) is independent of the type of basis functions used. Such spin distribution stems therefore from the principles of quantum mechanics and should be amenable to experimental determination.

In the case of a tetrahedral compound with one unpaired electron, having the $e^4 t_2^5$ electron configuration (Fig. 2), all the features discussed for the two previous cases show up: (a) a four-lobe orbital shape centered at the metal atom, (b) no spin density at the ligands that are in the nodal plane, (c) positive spin density at the ligands that interact in a σ^* way with the metal and (d) spin density minima along these bonds. In addition, in this case we can also observe an asymmetry in the lobes of the metal spin density resulting from the hybridization of d and p orbitals that minimizes the metal–ligand antibonding character of the SOMO (**5**).

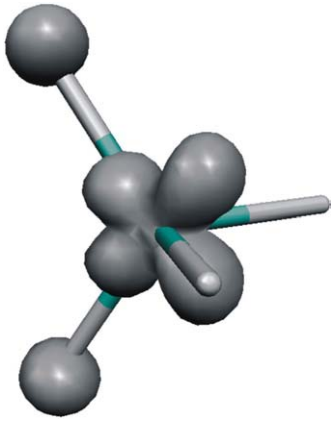

Fig. 2. Representation of the isodensity surface (cutoff of 0.02 electron/bohr^3) of the spin density distribution for a tetrahedral d^9 complex with σ-donor ligands. Gray shapes correspond to positive spin densities.

5 6

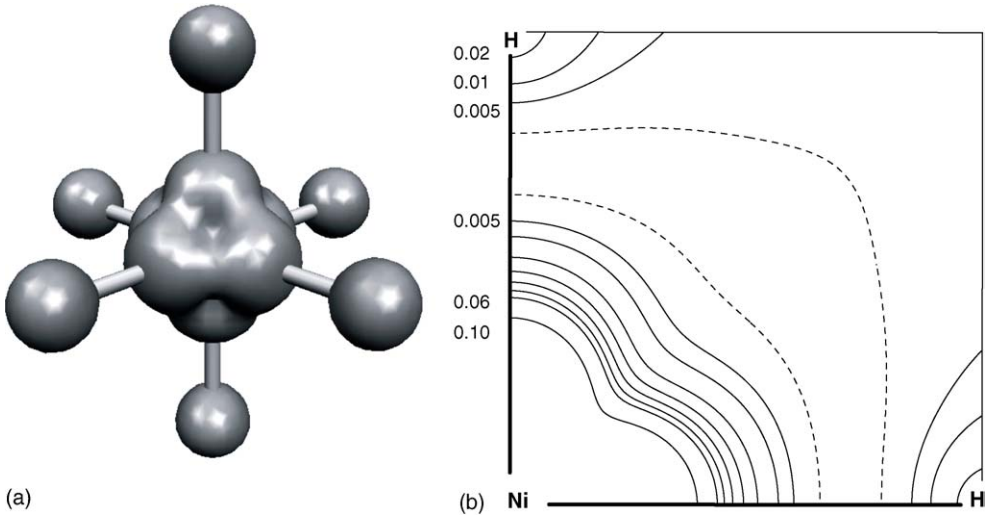

Fig. 3. Representation of the isodensity surface (a) and contour map (b) of the spin density distribution for an octahedral d^8 complex with σ-donor ligands. Gray shapes of the isodensity surface correspond to positive spin densities (cutoff of 0.01 used); the following isodensity lines are plotted in the contour map: 0.10, 0.06, 0.05, 0.04, 0.03, 0.02, 0.01, 0.005 and 0.000 (dashed line). Minute negative values of the spin density are found between the two zero lines.

The next group of configurations to consider are those in which only the e orbitals (strictly speaking, e_g in the octahedral case) are partially occupied. For the octahedral case ($t_{2g}^6 e_g^2$ configuration, Fig. 3a), the spin density has the form of an octahedron with empty faces, that can be easily understood as a combination of the shapes of the two e_g orbitals that have lobes in the direction of the six ligands (i.e., of the six vertices of the octahedron). Because of the significant delocalization of the e_g electrons onto the ligands, positive spin density appears at the donor atoms and, again, minima in the spin density distribution appear approximately at the midpoint of the metal–ligand bonds. The octahedral shape of spin density in the e_g^2 configuration and the cubic form of that of the t_{2g}^3 has been noted previously by us [39]. The fact that spin delocalization presents a gap along the metal–ligand bonds is associated with the presence of nodal planes in the metal–ligand antibonding e_g orbitals and can be best appreciated in the corresponding contour plot (Fig. 3b).

Similarly, the spin density distribution of a tetrahedral e^2 ion (Fig. 4a) has the shape of an undistorted octahedron, since these d orbitals do not mix with those of the σ-donor ligands because the metal–ligand bonds are in their nodal surfaces (**6**). The vertices of such a spin octahedron are directed to the edge centers of the molecular tetrahedron, providing a nice example of the relationship between these two Platonic figures [37]. If we look at the finer details by plotting the isodensity surface of a much smaller value of the spin population (Fig. 4b), we can detect the existence of small pear-shaped regions of negative spin density at the ligands that must be attributed to spin polarization.

Let us focus now on those cases in which all the orbitals of a t_2 set are occupied with unpaired electrons, i.e., the octahedral t_{2g}^3 and tetrahedral $e^4 t_2^3$ configurations. In the first case (Fig. 5a), in which the t_{2g} orbitals do not interact with the σ-donor ligands, the spin density of the t_{2g}^3 configuration is concentrated along the directions of the lobes of those orbitals, i.e., from the center to the faces of the octahedron, resulting in the shape of the dual of the octahedron, a cube, with holes at the face centers. These holes correspond to the directions of intersection of the nodal planes of the three t_{2g}

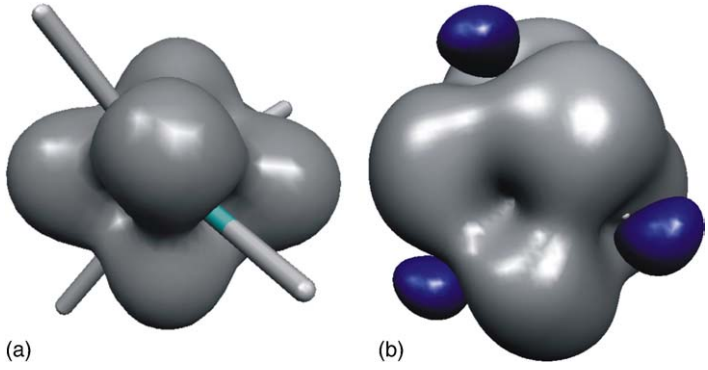

Fig. 4. Representation of two isodensity surfaces of the spin density distribution for a tetrahedral d^2 complex with σ-donor ligands. Gray shapes correspond to positive spin densities. The cutoff values used for these drawings were 0.02 (a) and 0.0005 (b).

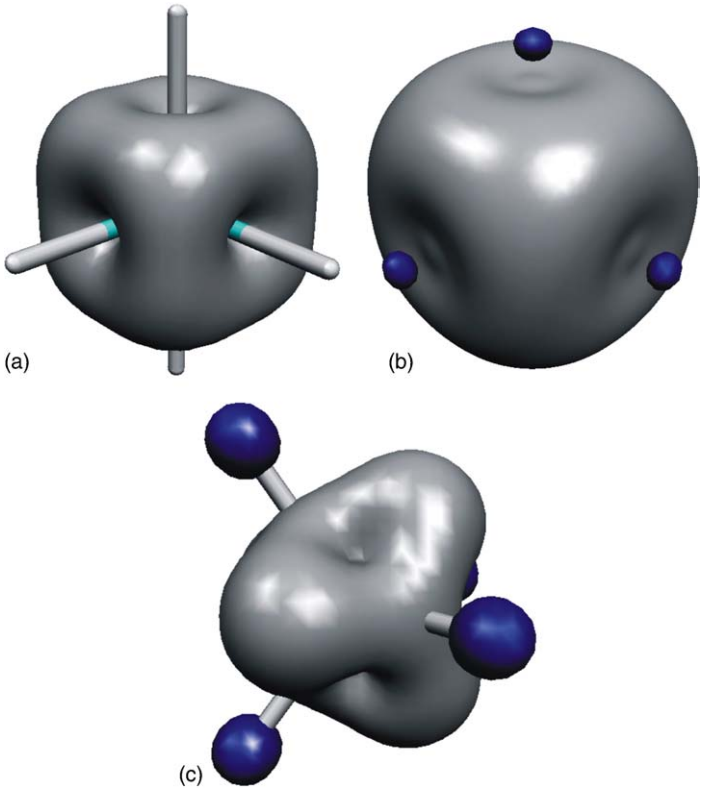

Fig. 5. Representation of the isodensity surface of the spin density distribution for an octahedral d^3 (a and b) and a tetrahedral d^7 complex with σ-donor ligands (c). Gray shapes correspond to positive, dark shapes to negative spin densities. The cutoff values used for these drawings were 0.02, 0.0007 and 0.01, respectively.

orbitals, for which the probability of finding the unpaired electrons is zero. One has to look at much smaller values of the spin density (Fig. 5b) to detect two subtle effects, the appearance of negative spin at the ligand atoms due to spin polarization, and the existence of a non-negligible spin along the nodal metal–ligand directions introduced by the polarization functions used in the calculations. In a tetrahedral compound with the related $e^4t_2^3$ configuration, the shape of the electron density distribution is again approximately that of a cube, even if significantly distorted (Fig. 5c). Four vertices of the spin cube appear along the metal–ligand bonds and the remaining four point to the centers of the tetrahedral faces. However, the SOMOs have smaller probabilities in the direction of the metal–ligand bonds, as seen in the orbital hybridization schematized in **5**, the spin densities are smaller in those directions than in the directions of the faces, and the spin cube appears squeezed along the former four vertices as can be appreciated in Fig. 5c. This shape can be understood as derived from that of the $e^2t_2^3$ configuration (see Fig. 6c) by removing the spin density corresponding to the e orbitals, which are directed to the centers of the tetrahedral edges, thus producing the marked pits along those directions.

We can conclude our selection of characteristic shapes of the metal spin densities with those systems in which all five valence d orbitals bear an unpaired electron. For the d^5 electron configuration in a free metal atom, a spherical distribution of the spin density should be expected. In the case of the octahedral complex with a $t_{2g}^3e_g^2$ configuration, the isodensity surface (Fig. 6a) has indeed approximately the shape of a sphere centered at the Mn atom, even if somewhat flattened in the directions of the metal–ligand bonds. It is nice to see how the combination of the octahedral shape of the e_g^2 spins (Fig. 3a) and the cubic shape of the t_{2g}^3 ones (Fig. 5a) discussed above results in the nearly spherical shape of the spin density for a $t_{2g}^3e_g^2$ configuration. The loss of sphericity is magnified if we look at a lower density surface (Fig. 6b), resulting in nearly a cube with pits in the faces, combined with the appearance of small positive spin density at the ligands due to delocalization of the e_g orbitals. It is also interesting to observe again that there is a region between the metal and ligand atoms in which no spin density can be found at the low cutoff value chosen, nicely revealing the nodes of the antibonding e_g orbitals, as discussed above for the d^8 case.

In a d^5 tetrahedral complex ($e^2t_2^3$ configuration), the sphericity is also lost in part (Fig. 6c), due to flattening along the metal-distance bonds. However, the spin density at the ligands is in this case negative, given the formally non bonding character of the metal d orbitals consistent with an sp^3 hybridization. Hence, the predominance of spin polarization of the ligands' lone pairs over spin delocalization is responsible for their net negative spin density. The flattening of the sphere along the bond directions, much more pronounced

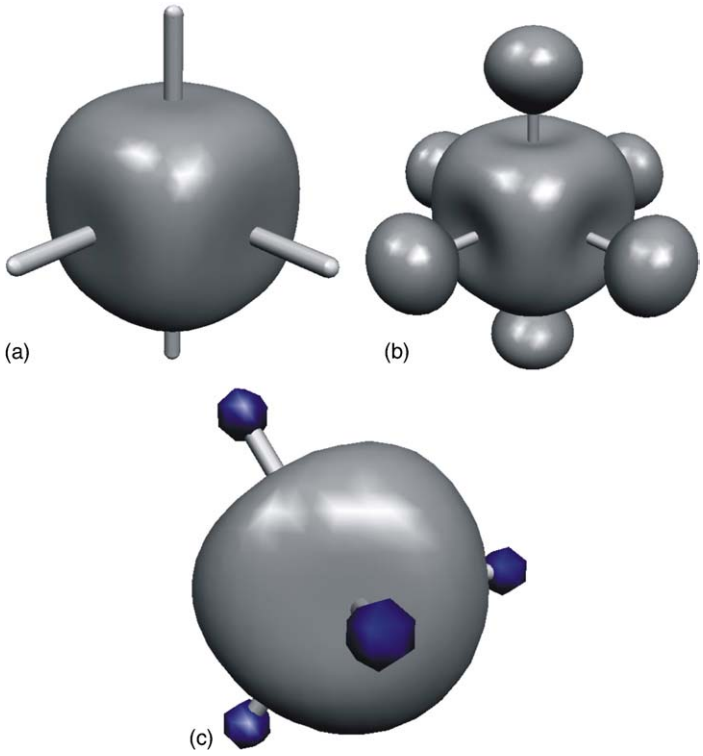

Fig. 6. Representation of the isodensity surface of the spin density distribution for an octahedral high spin d^5 (a and b) and a tetrahedral d^5 complex with σ-donor ligands (c). Gray shapes correspond to positive, dark shapes to negative spin densities. The cutoff values used for these drawings were 0.02, 0.005 and 0.02, respectively.

than in the octahedral analogue, is the result of significant hybridization of the t_2 orbitals (see **5**) that decrease the probability of the corresponding unpaired electrons in those regions of space. The negative spin at the ligands due to polarization is larger in the $e^4t_2^3$ than in the $e^2t_2^3$ case shown above, consistent with the coexistence of e-spin delocalization and t_2-spin polarization in a d^5 ion.

Some scattered examples exist in the literature in which the spin shapes just discussed can be recognized, although these come mostly from computational studies, since PND spin distribution maps are usually shown only as contour plots in one molecular plane, not in a tridimensional perspective. Thus, in a vanadyl-copper(II) dinuclear complex assembled through hydrogen bonds, the shapes of the two orthogonal d orbitals can be clearly appreciated (Fig. 7a), combined with the negative spin at the vanadyl oxo atom due to spin polarization and the positive density at the atoms coordinated to Cu(II) due to spin delocalization [41]. A similar system with Cr(III) and Ni(II) centers shows also the spin density shapes described above for simpler models with the same electron configurations (Fig. 7b). Another example can be found in a dinuclear complex in which two Cr(III) ions are connected through very long bridges, that show nicely the cubic spin density expected for the t_{2g}^3 configuration (Fig. 8), together with the spread of positive and negative spin densities throughout the π system of the bridging ligand [42].

Other depictions of spin densities at metal centers that can be found in the literature correspond to hydrogen-bridged

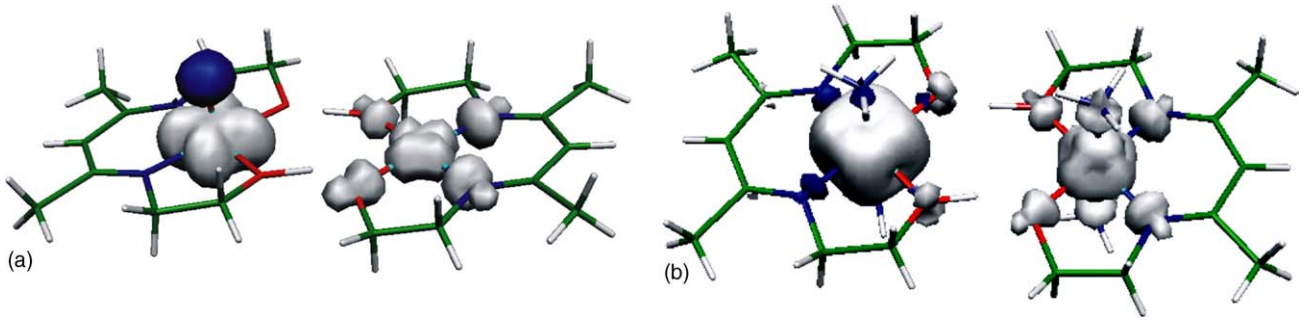

Fig. 7. Representation of the spin density distribution for hydrogen-bonded assemblies of a vanadyl and a Cu(II) complexes (a) and Cr(III) and Ni(II) complexes (b). White shapes correspond to positive, dark shapes to negative spin densities. Reproduced from Ref. [41] with permission from the Royal Society of Chemistry.

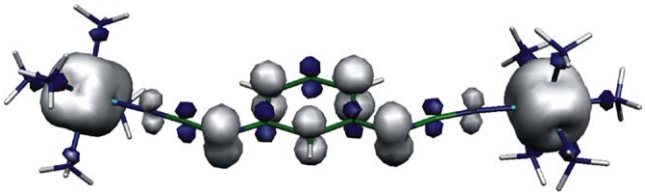

Fig. 8. Spin density distribution for a dinuclear Cr(III) complex with a long bridging ligand. White shapes correspond to positive, dark shapes to negative spin densities. Reproduced from Ref. [42] with permission from the American Chemical Society.

Cu(II) complexes [39] and to the excited triplet state of the dinuclear Pt(II) complex with pyrophosphato bridges [43] that nicely reveals the metal–metal σ character of the HOMO and LUMO.

Among polynuclear transition metal complexes, much attention is being paid recently to systems with high total spin, the most interesting ones being those exhibiting single molecule magnet (SMM) behavior. The reported spin density maps for those compounds can be easily understood by superimposing the shapes expected for mononuclear complexes, as discussed above, and nicely reflect the existence of ferro- or antiferromagnetic interactions. A large spin ($S = 39/2$) molecule with the Mn_9Mo_6 metal core has been shown to provide a whole catalog of spin shapes [44] in its spin density map (Fig. 9). Besides the characteristic features of this map that can be interpreted as resulting from the interplay between spin delocalization and spin polarization [14], one can identify the shape of a d_{xy} orbital at each Mo atom, that of the p orbitals of the C and N atoms of cyanide bridges, nearly spherical spin distributions around the Mn(II) ions, the shape of an sp^3 hybrid orbital of the O atoms of a terminal methanol ligands and the shape of an sp hybrid at the N atoms of the bridging cyanides. The coexistence of positive σ and negative π spin density at the same metal atom is another remarkable feature of the complex electronic structure of Mn_9Mo_6.

As for the first compound reported to present SMM behavior, an acetato Mn_{12} compound, ^{55}Mn NMR spectroscopy [45], polarized neutron diffraction [46] and XMCD [11] studies confirm the description of its $S = 10$ ground state as resulting from spin moments of the inner four Mn^{4+} ions ($S = 3/2$) antiparallel to those of the eight outer Mn^{3+} ions ($S = 2$). Complementary information from ^{13}C NMR spectroscopy demonstrates that significant spin delocalization can be found at the methyl groups of the acetato ligands, amounting to some 1.6% of the total spin density of the molecule [47]. The spin density distribution in a Fe_8 SMM with $S = 10$ has been studied by PND [48], although the strong asymmetry observed in the magnetic moments of the different Fe(III) ions is not substantiated by the calculated spin density map [49]. For the same compound, a 0.3% of the unpaired electron density in the Fe_8Br_8 cluster was estimated to reside at the Br atoms, according to a ^{81}Br NMR study [50]. A full spin density map, obtained via DFT calculations, has also been reported recently for an Fe_{11} SMM compound [51].

5. Conclusions

The spin density distribution throughout a molecule of a paramagnetic coordination compound can be obtained from experimental techniques such as NMR spectroscopy, polarized neutron diffraction or X-ray magnetic circular dichroism, and can also be estimated to a good approximation by means of theoretical calculations. The use of hybrid density

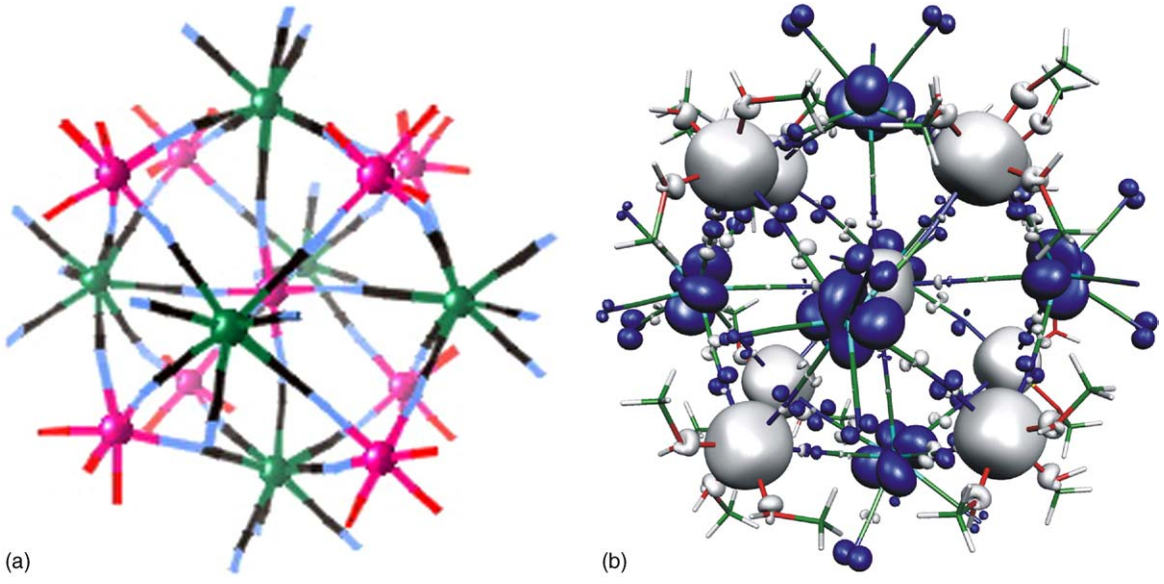

Fig. 9. Molecular structure (a) and spin density of the $S = 39/2$ ground state of a Mn_9Mo_6 complex (b). Dark and light spheres represent Mn and Mo atoms, respectively; sticks represent bonds to N, C and O atoms. The carbon atoms of the methanol ligands are omitted for clarity. In the spin density map, clear and dark regions indicate positive and negative spin populations, respectively). Reproduced with permission from Ref. [44].

functionals seems to provide the most cost effective means for such calculations, whereas the method used for population analysis (Mulliken, NBO or AIM) does not seem to have a significant influence on the results. The use of pseudopotentials, though, modifies in a quantitatively significant way the calculated spin density distribution, although at present time there seems to be neither a clear explanation nor systematic trends for such an effect.

Examples of the interplay between spin polarization and spin delocalization in determining the spin density distribution in dinuclear complexes are given, which can be mostly understood as the superposition of the spin densities of the hypothetical mononuclear parents.

The systematic analysis of the shapes of spin densities around a transition metal atom indicate that these can appear as spheres, cubes, octahedra, tetrahedra or four-lobed shapes, depending on the electron configuration of the metal, in a predictable way. Small deviations from such ideal figures can be understood by taking into account delocalization effects. An advantage of studying spin density distributions compared to electron densities is that the large part of the electron density corresponding to the atomic cores do not mask the unpaired valence electrons. A remarkable finding is that in specific cases, even if an unpaired electron residing in a metal atom is delocalized toward a ligand, a region of zero spin density appears along the metal–ligand bond.

Acknowledgments

Financial support to this work was provided by DGES, project PB95-0848. J. Cirera thanks MEC for a doctoral grant. The authors thank an anonymous referee for pointing to some recent references reporting NMR-derived spin densities of polynuclear complexes.

References

[1] G.N. La Mar, J. Horrocks, W. DeW, R.H. Holm, NMR of Paramagnetic Molecules, Academic Press, New York, 1973.
[2] L. Banci, M. Piccioli, A. Scozzafava, Coord. Chem. Rev. 150 (1992) 29.
[3] R.S. Drago, Physical Methods for Chemists, Saunders, Orlando, FL, 1992.
[4] I. Bertini, C. Luchinat, Coord. Chem. Rev. 150 (1996) 29.
[5] L.J. Berliner, J. Reuben (Eds.), NMR of Paramagnetic Molecules;, Plenum Press, New York, 1993.
[6] J.A. Weil, J.R. Bolton, J.E. Wertz, Electron Paramagnetic Resonance, Wiley, New York, 1994.
[7] B. Gillon, J. Schweizer, in: J. Maruani (Ed.), Molecules in Physics, Chemistry and Biology, vol. 2, Kluwer Academic, Dordrecht, 1989, pp. 111–147.
[8] R.J. Papoular, E. Ressouche, J. Schweizer, A. Zheludev, in: A. Mohammad-Djafari, G. Demoment (Eds.), Maximum Entropy and Bayesian Methods, vol. 53, Kluwer Academic, Dordrecht, 1993, p. 311.
[9] P. Sainctavit, C. Cartier dit Moulin, M.A. Arrio, in: J.S. Miller, M. Drillon (Eds.), Magnetism: Molecules to Materials, vol. 1, Wiley/VCH, Weinheim, 2001, pp. 131–153.
[10] G. Champion, M.-A. Arrio, P. Sainctavit, M. Zacchinga, M. Zangrando, M. Finazzi, F. Parmigiani, F. Villain, C. Mathonière, C. Cartier dit Moulin, Monats. Chem. 134 (2003) 277.
[11] R. Moroni, C. Cartier dit Moulin, G. Champion, M.A. Arrio, P. Sainctavit, M. Verdaguer, D. Gatteschi, Phys. Rev. B 68 (2003) 64407.
[12] M. Gillon, in: J.S. Miller, M. Drillon (Eds.), Magnetism: Molecules to Materials, vol. 1, Wiley/VCH, Weinheim, 2001, pp. 357–378.
[13] F. Kohler, in: J.S. Miller, M. Drillon (Eds.), Magnetism: Molecules to Materials, vol. 1, Wiley/VCH, Weinheim, 2001, pp. 379–430.
[14] J. Cano, E. Ruiz, S. Alvarez, M. Verdaguer, Comments Inorg. Chem. 20 (1998) 27.
[15] W. Koch, M.C. Holthausen, A Chemist's Guide to Density Functional Theory, 2nd ed., Wiley/VCH Verlag, Weinheim, 2001.
[16] J.C. Slater, The Self-consistent Field for Molecules and Solids, vol. 4, McGraw-Hill, New York, 1974.
[17] S.H. Vosko, L. Wilk, M. Nusair, Can. J. Phys. 58 (1980) 1200.
[18] A.D. Becke, Phys. Rev. A 38 (1988) 3098.
[19] C. Lee, W. Yang, R.G. Parr, Phys. Rev. B 37 (1988) 785.
[20] A.D. Becke, J. Chem. Phys. 98 (1993) 5648.
[21] G.S. Chandler, G.A. Christos, B.N. Figgis, P.A. Reynolds, J. Chem. Soc., Faraday Trans. 88 (1992) 1961.
[22] E. Ressouche, J. Schwizer, in: W. Linert, M. Verdaguer (Eds.), Molecular Magnets: Recent Highlights, Springer, New York, 2003, pp. 119–137.
[23] A.E. Reed, L.A. Curtiss, F. Weinhold, Chem. Rev. 88 (1988) 899.
[24] R.F.W. Bader, Atoms in Molecules: A Quantum Theory, Oxford University Press, Oxford, 1990.
[25] M. Gillon, C. Mathonière, E. Ruiz, S. Alvarez, A. Cousson, O. Kahn, J. Am. Chem. Soc. 124 (2002) 14433.
[26] J.J. Novoa, P. Lafuente, M. Deumal, F. Mota, in: J.S. Miller, M. Drillon (Eds.), Magnetism: Molecules to Materials IV, vol. 4, Wiley/VCH, Weinheim, 2003, p. 65.
[27] B.N. Figgis, J.B. Forsyth, P.A. Reynolds, Inorg. Chem. 26 (1987) 101.
[28] Y.-P. Liu, J. Chem. Inf. Comput. Sci. 41 (2001) 22.
[29] E. Ruiz, A. Rodríguez-Fortea, T. Cauchy, J. Tercero, C. Massobrio, submitted for publication.
[30] A. Schaefer, H. Horn, R. Ahlrichs, J. Chem. Phys. 97 (1992) 2571.
[31] M.A. Aebersold, M. Gillon, O. Plantevin, L. Pardi, O. Kahn, P. Bergerat, I.F.T. von Seggern, L. Öhrström, A. Grand, E. Lelièvre-Berna, J. Am. Chem. Soc. 120 (1998) 5238.
[32] E. Ruiz, J. Cano, S. Alvarez, P. Alemany, J. Am. Chem. Soc. 120 (1998) 11122.
[33] J. Cano, E. Ruiz, P. Alemany, F. Lloret, S. Alvarez, J. Chem. Soc., Dalton Trans. (1999) 1669.
[34] B. Gillon, C. Mathonière, E. Ruiz, S. Alvarez, A. Cousson, T.M. Rajendiran, O. Kahn, J. Am. Chem. Soc. 124 (2002) 14433.
[35] Y. Pontillon, A. Bencini, A. Caneschi, A. Dei, D. Gatteschi, B. Gillon, C. Sangregorio, J. Stride, F. Totti, Angew. Chem., Int. Ed. Engl. 39 (2000) 1786.
[36] J. Itatani, J. Levesque, D. Zeidler, H. Niikura, H. Pépin, J.C. Kieffer, P.B. Corkum, D.M. Villeneuve, Nature 432 (2004) 867.
[37] S. Alvarez, Dalton Trans., in press.
[38] The calculation of spin density shown was performed with the CPMD code (Car Parrinello Molecular Dynamics, version 3.7.2) with the hybrid B3LYP functional recently implemented in this code and using norm conserving pseudopotentials to account for core–valence interactions.
[39] C. Desplanches, E. Ruiz, A. Rodríguez-Fortea, S. Alvarez, J. Am. Chem. Soc. 124 (2002) 5197.
[40] E. Ruiz, A. Rodríguez-Fortea, S. Alvarez, M. Verdaguer, Chem. Eur. J. 11 (2005) 2135.
[41] C. Desplanches, E. Ruiz, S. Alvarez, Chem. Commun. (2002) 2614.
[42] E. Ruiz, A. Rodríguez-Fortea, S. Alvarez, Inorg. Chem. 42 (2003) 4881.

[43] I.V. Novozhilova, A.V. Volkov, P. Coppens, J. Am. Chem. Soc. 12 (2003) 1079.
[44] E. Ruiz, G. Rajaraman, S. Alvarez, B. Gillon, J. Stride, R. Clérac, J. Larionova, S. Decurtins, Angew. Chem., Int. Ed. Engl. 44 (2005) 2711.
[45] Y. Furukawa, K. Watanabe, K. Kumagai, F. Borsa, D. Gatteschi, Phys. Rev. B 64 (2001) 104401.
[46] R.A. Robinson, P.J. Bronw, D.N. Argyriou, D.N. Hendrickson, S.M.J. Aubin, J. Phys.: Condens. Matter 12 (2000) 2805.
[47] R.M. Achey, P.L. Kuhns, A.P. Reyes, W.G. Moulton, N.S. Dalal, Solid State Commun. 121 (2002) 107.
[48] Y. Pontillon, A. Caneschi, D. Gatteschi, R. Sessoli, E. Ressouche, J. Schweizer, E. Lelievre-Berna, J. Am. Chem. Soc. 121 (1999) 5342.
[49] E. Ruiz, J. Cano, S. Alvarez, Chem. Eur. J. 11, in press.
[50] D. Zipse, J.M. North, R.M. Achey, N.S. Dalal, S. Hill, R.S. Edwards, E.S. Choi, J.S. Brooks, J. Appl. Phys. 95 (2004) 6900.
[51] E. Ruiz, J. Cano, S. Alvarez, Polyhedron, in press.
[52] A. Schaefer, C. Huber, R. Ahlrichs, J. Chem. Phys. 100 (1994) 5829.